Nanoscale

PAPER

View Article Online
View Journal | View Issue

Cite this: *Nanoscale*, 2021, **13**, 10061

Highly stable graphene oxide composite nanofiltration membrane†

Kaiqiang Zheng,[a] Shiqing Li,[a] Zhou Chen, *[a] Yunqiang Chen,[b] Yubin Hong*[b] and Weiguang Lan*[a,b]

Received 23rd March 2021,
Accepted 7th May 2021

DOI: 10.1039/d1nr01823j

rsc.li/nanoscale

Graphene oxide (GO) based membranes are promising for advanced nanofiltration in water treatments but there is a need to improve water flux and membrane stability. Although the interlayer distance of GO membranes can be expanded using intercalants to improve permeability, achieving uniform intercalation without the added complication of water-induced swelling is challenging. Herein, we report the fabrication of GO hybrid lamellar membranes with controllable layer structures to achieve high performance in nanofiltration. The interlayer spacing of the GO hybrid membrane is regulated using TiO_2 intercalants of different sizes, while the stability of GO membranes is enhanced by encapsulating with polyethyleneimine (PEI). The optimal composite membrane delivers a pure water-flux up to 26.0 L m^{-2} h^{-1} bar^{-1} with a 99.9% rejection of methylene blue and eosin under an ultra-low pressure nanofiltration condition. More importantly, the composite membrane sustains good cycling stability after 5 filtration cycles of dye, which enables the potential industrial application in realizing ultra-stable GO based membranes.

1. Introduction

The development of cost-effective and sustainable technologies for water treatment is of paramount importance to solve the water crisis and ensure clean and safe drinking water. As an eco-friendly and energy-saving technology, membrane filtration is playing an increasingly important role in water treatment technology.[1–4] Nanofiltration (NF) membranes with a pore size smaller than 0.001 microns are highly useful for resource conservation and cleaner production in many industrial fields, spanning from desalination,[5–8] organic matter removal,[9,10] and pharmaceuticals[11–14] to petrochemicals.[15,16] The design of materials with tunable structural composition and configuration is critical for the advancement of NF performance. Currently, most NF membranes are composed of polymer-based materials, which usually suffer from a well-known trade-off between permeability and selectivity. There is an ongoing worldwide effort to search for next-generation NF materials.

Recent improvements in graphene oxide (GO) based membranes have aroused great interest in the field of water and gas purification because of their inherent structural advantages, including two-dimensional (2D) lamellar structure and tailorable functional groups on the nanosheet edges and frictionless flow of water molecules on the non-oxidized sp^2 graphene region.[17–19] Unfortunately, the low permeance of GO based membranes hamper their practical application. In addition, the stability of the GO membrane degrades rapidly when operated under harsh environmental conditions, such as high water pressure or ion concentrations, owing to the compression of the interlayer galleries.[20,21] One way to improve the permeance is by inserting intercalation materials into the interlayer gallery to counteract the compression of the membrane at high pressure. To date, a lot of intercalated materials have been widely investigated, including multi-walled carbon nanotubes (MWCNTs),[22,23] single-walled carbon nanotube (SWCNTs),[24] polyelectrolytes,[25] inorganic nanoparticles (NPs),[26] and metal–organic frameworks.[27,28] The motivation for using an intercalant is to maintain the structural integrity of the membrane while the interlayer distance of GO membrane is enlarged. For example, Jiang *et al.* studied the insertion of CNTs in GO to make tunable nanochannels, achieving the water permeability of 52.7 L m^{-2} h^{-1} bar^{-1} and attaining 100% rejection efficiency for different charged organic dyes.[22] Xu *et al.* prepared an NF membrane composite by ultrasonically mixing GO with dopamine-modified TiO_2, and the hybrid membrane was crosslinked using dopamine hydrochloride and polyethyleneimine to improve the permeance (up to 41.6 L m^{-2} h^{-1} bar^{-1}).[29] In addition, the *d*-spacing of graphene oxide-framework (GOF) layers was adjusted from 8.7 to 10.4 Å by crosslinking diamines, as proposed by Hung *et al.* The 1,4-cyclohexanediamine (CDA)-modified GO composite membrane

[a]*Xiamen University Center for Membrane Application and Advancement, College of Materials, Xiamen University, Xiamen 361005, Fujian, China. E-mail: zhouchen@xmu.edu.cn*
[b]*Suntar Membrane Technology (Xiamen) Co., Ltd., Xiamen 361022, Fujian, China*
†Electronic supplementary information (ESI) available. See DOI: 10.1039/d1nr01823j

achieved a water flux of 20.1 L m^{-2} h^{-1} with ion rejection of 99.9% for desalination of 3.5 wt% seawater at 90 °C.[25] However, in all cases, the intercalation of the GO interlayer reduces the mechanical integrity of the enlarged laminate structure, negatively affecting its separation and stability.

The poor stability of the GO based membrane is a major issue hampering practical application. The presence of hydrophilic functional groups on the edge and the negative charge of the GO membrane increase water flux but also make it prone to re-dispersion, leading to poor durability under aqueous conditions.[18] The GO membrane could be partially reduced to reduced graphene oxide (rGO) to decrease the hydrophilic groups and charge properties, and thus alleviate the re-dispersion issue.[30] In addition, metal ions[31] and amide bonds[32] have also been introduced to cross-link GO interlayers and mitigate the instability issue. Although these strategies have mitigated the redispersion problem of GO lamellae in aqueous solutions and improved the membrane stability to some extent, they have inevitably increased the resistance to interlayer flow and lowered the water flux.

To achieve the combined properties of high permeance and stability in GO-based membranes, we propose a two pronged approach: adding an intercalant between the GO interlayers and cross-linking with a membrane cortex. A hydrothermal synthesis method was used to uniformly load TiO_2 on GO lamellae.[33] The interlayer distance of the GO membrane can be regulated by the size of the TiO_2 nanocrystals. Besides, the surface properties of the GO membrane were adjusted by grafting the hydrophilic polycationic polyetherimide (PEI) molecules on the surface layer of the membrane. Electrostatic interactions and hydrogen bonds between GO and PEI can be adjusted by changing the branching chain length of PEI with different molecular weights (MWs). Under ultra-low pressure, the optimally tuned composite membrane exhibits the best separation performance with a pure water permeance of 26 L m^{-2} h^{-1} bar^{-1} and 99.9% rejection of anionic eosin dye and cationic methylene blue dye. The relationship between the physicochemical properties of synthesized GO hybrid membranes and their performance was systematically investigated. Our findings represent a reliable way to make stable GO composite membranes for high flux water filtration.

2. Experimental part

2.1 Materials

Natural flake graphite (455 mesh) and eosin-Y were purchased from Sinopharm Chemical Reagent Co. Ltd (China). Concentrated sulfuric acid (H_2SO_4, 95%), potassium permanganate ($KMnO_4$), phosphoric acid (H_3PO_4, 85%), hydrogen peroxide (H_2O_2, 30%), hydrochloric acid (HCl, 98%), magnesium sulphate ($MgSO_4$, 99%), sodium sulphate (Na_2SO_4, 99%), magnesium chloride ($MgCl_2$, 95%) sodium chloride (NaCl, 99%) and methyl blue (MB) were purchased from XiLong Chemical Reagents Co. Ltd (China). Titanium sulfate ($Ti(SO_4)_2$, 96%) was obtained from Sigma-Aldrich (China). Cellulose acetate (CA, 0.45 μm) microporous support membrane (28.26 cm^2) was purchased from Shanghai Xinya purification device factory. Polyethyleneimine (PEI) with MWs of 600, 1800, 10 000 and 70 000 g mol^{-1} were purchased from Aladdin Industrial Co. Ltd (China). VNF1 and VNFK commercial membranes were purchased from Vontron Co. Ltd (China). DK commercial membrane was purchased from Ge Osmonics Co. Ltd (USA).

A detailed description of the preparation of the membrane, the characterization of the membrane and filtration testing are provided in the ESI.†

3. Results and discussion

3.1 Fabrication of a G-TX-PY composite membrane

The fabrication process of a G-TX-PY composite membrane is schematically illustrated in Fig. 1. Typically, a G-TX solution was filtered on the CA substrate membrane to get the G-TX membrane by a suction filtration method (Fig. 1a and b). To obtain the membrane with a bound cortex, a PEI solution was slowly poured on the surface of the G-TX membrane (Fig. 1c) and left to soak for 5 min and then suction filtration was applied to prepare the G-TX-PY composite membrane; the diagram of the bound cortex surface of G-TX-PY is shown in Fig. 1d. After keeping the G-TX solution one week (Fig. 1e), we found that GO, G-T2 and G-T3 solutions have good dispersion and smooth GO, G-T2 and G-T3 membranes can be prepared (Fig. 1f).

3.2 Morphology and physicochemical properties of GO and G-TX

The SEM morphologies of GO and G-TX nanosheets are shown in Fig. 2a and S3a.† Both GO and G-TX membranes show a 2D lamellar structure, demonstrating that the introduction of TiO_2 onto the GO nanosheets did not destroy the 2D structure of GO. The distribution and size of TiO_2 nanocrystals on G-TX changes with the concentration of $Ti(SO_4)_2$ used (as shown in

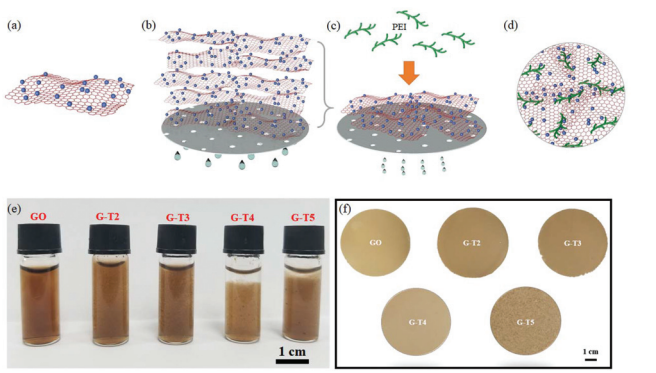

Fig. 1 Illustration of the preparation process of the GO composite membrane. The diagram of (a) G-TX lamellar structure, (b) G-TX based membrane, (c) grafting PEI on the G-TX membrane, (d) the surface of G-TX-PY composite membrane. (e) The digital photographs of GO and G-TX solution after storage for one week. (f) The optical photographs of GO and G-TX membranes.

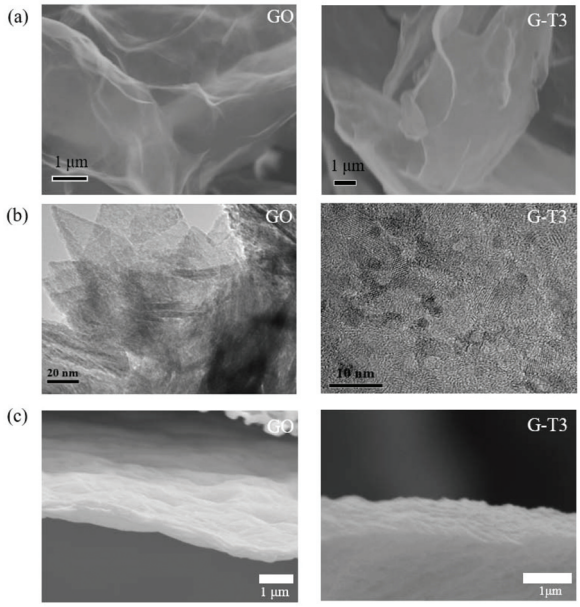

Fig. 2 (a) SEM, (b) TEM and (c) cross-sectional SEM images of GO and G-T3 membranes.

the TEM images in Fig. 2b and S3b†). TiO_2 nanocrystals are uniformly dispersed on the GO nanosheets at a low $Ti(SO_4)_2$ concentration (G-T2 and G-T3 membranes), while a high concentration of $Ti(SO_4)_2$ results in the aggregation of TiO_2 in the G-T4 and G-T5 membranes. Therefore, the thickness of GO composite membranes can be adjusted by changing the size of TiO_2 intercalants. The cross-section SEM images of G-TX membranes were recorded to directly visualize the thickness and stacking states of composite membranes (Fig. 2c and S3c†). Interestingly, the interlayers of the GO, G-T2, G-T3 composite membranes are neatly arranged, while the interlayer arrangements for G-T4 and G-T5 are more disordered. Clearly, the average thickness value is linearly dependent on the size of TiO_2 (Fig. S4†). Besides, the weight content of TiO_2 increased from 38.7% for G-T2 to 55.1% for G-T5 according to TGA (Fig. S5†). Therefore, the distribution and size of TiO_2 nanoparticles regulate the interlayer thickness of G-TX membranes.

The XRD patterns of GO and G-TX are shown in Fig. 3a. A diffraction peak of around 10.1° is ascribed to the (100) reflection of GO with an interlayer spacing of 0.88 nm,[31,34,35] which is higher than that of pristine graphite (0.34 nm).[36] For the G-TX membranes, the XRD peaks of around 26.1°, 37.4°, 48.3°, 54.8° can be assigned to the (101), (004), (200) and (105) crystal faces of TiO_2, respectively.[37] It should be emphasized that the characteristic (002) peak of GO disappeared after loading TiO_2, evidencing that introducing TiO_2 could adjust the interlayer spacing of the G-TX membrane.

The interlayer distance of the GO membrane affects the water flux and dye rejection performance. To verify the relationship between the size of TiO_2 and NF performance, MB was selected as the model rejection dye. We then measured the pure water flux and MB rejection performance of the G-TX based membranes under 1 bar (Fig. 3b). Obviously, the pure water flux of the G-TX membrane is proportional to the size of TiO_2. The large TiO_2 particles break the parallel arrangement between GO lamellae, resulting in losing the steric hindrance effect toward the rejection of MB. Among the G-TX membranes, the optimal G-T3 membrane exhibits a pure water flux of 25.9 L m^{-2} h^{-1} bar^{-1} (96 times higher than that of pristine GO membrane (0.27 L m^{-2} h^{-1} bar^{-1})) and an MB interception rate of nearly 100%, while TiO_2-rich membranes exhibit a lower rejection rate toward MB. Therefore, we selected the G-T3 membrane for further modification and investigated the effect of PEI encapsulation.

3.3 Morphology and physicochemical properties of G-T3-PY

The surface properties of a membrane are highly related to its mechanical integrity. Regulating the surface properties of the G-T3 membrane by grafting differently branched PEI is one effective solution we have adopted. The PEI-modified membranes do not change the gullied surface (Fig. S6†). However, for G-T3-P3 and G-T3-P4, the surface morphology becomes tighter, indicating that they would have a strong membrane structure and the potential to improve the mechanical integrity of the membrane under harsh conditions.

The FT-IR, XPS and depth XPS studies (ESI Fig. S7–S10†) support that the surface of the G-T3-PY membranes was successfully modified by PEI. Therefore, it is reasonable to anticipate that the surface hydrophilicity of PEI-modified membranes has been changed. A clear evidence is that the water contact angle (WCA) reduced with increased MW of PEI (Fig. 4). This is because a high MW PEI has more proportion

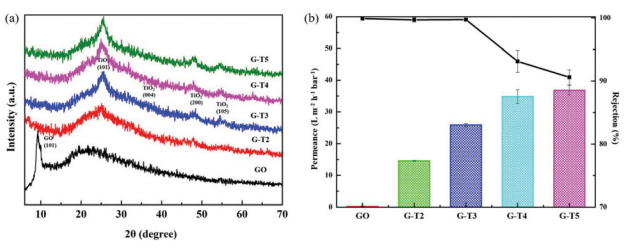

Fig. 3 (a) The XRD patterns and (b) water flux and MB retention of GO and G-TX based membranes.

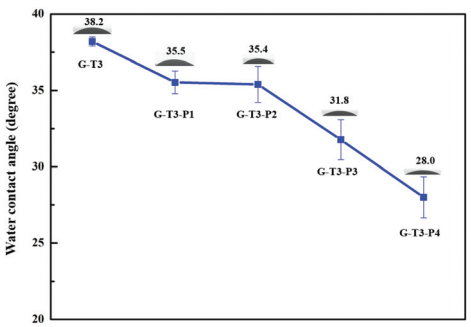

Fig. 4 WCA values of G-T3 and G-T3-PY membranes.

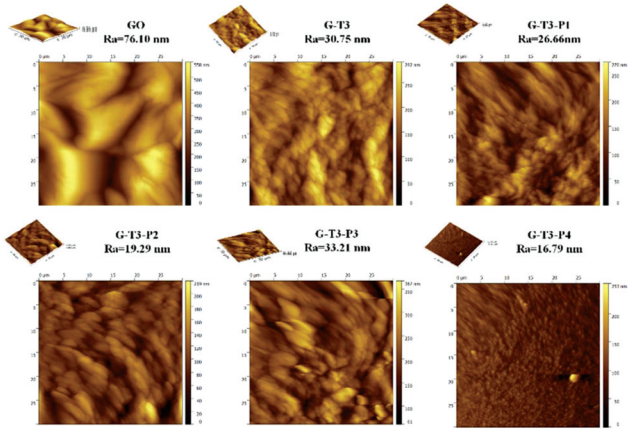

Fig. 5 AFM images of GO and G-T3-PY membranes. Inset is the R_a of corresponding membranes.

of hydrophilic amino groups, which endows it with good hydrophilicity.[38] In addition, the PEI-modified membranes exhibits smooth surface as verified by the roughness value (R_a) (Fig. 5). It is worth noting that a hydrophilic surface with a low R_a is beneficial for forming a hydration layer, which will prevent the adsorption of organic pollutants and thus improve the durability of the composite membrane.[39,40] In addition, the pore sizes of the GO membrane and G-T3-P4 composite nanofiltration membrane were characterized, and the calculated average pore size of the GO and G-T4-P3 membranes is about 2.12 and 3.15 nm, respectively (Fig. S11†).

3.4 Separation performance of membranes toward different ionic dyes

The pure water flux and dye retention performance of G-T3, G-T3-PY, VNF1, VNFK and DK membranes are shown in Fig. 6.

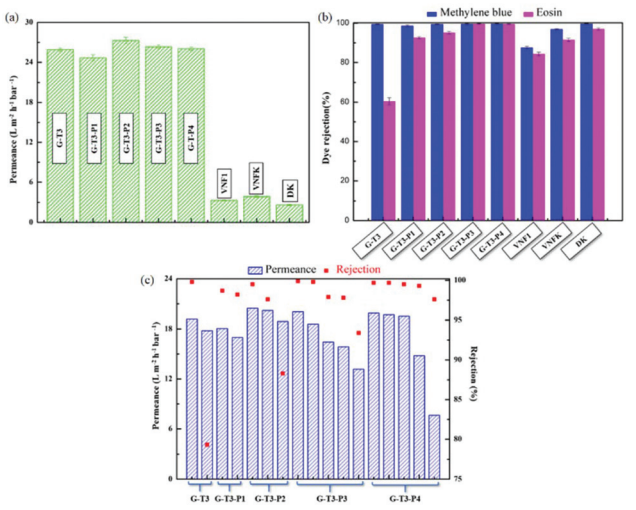

Fig. 6 (a) Pure water flux and (b) dye interception of G-T3, G-T3-PY, VNF1, VNFK and DK membranes. (c) Durability of G-T3 and G-T3-PY membranes.

Interestingly, the water flux of the PEI-modified membranes was improved. As shown in Fig. 6a, the pure water flux for G-T3, G-T3-P1, G-T3-P2, G-T3-P3, G-T3-P4, VNF1, VNFK and DK membranes is 25.9, 24.7, 27.3, 26.3, 26.0, 3.3, 3.9 and 2.6 L m^{-2} h^{-1} bar^{-1}, respectively. The water flux of the G-T3-P4 membrane is nearly 7 times higher than that of three commercial membranes. We further tested the rejection rate of the anionic eosin dye and cationic MB dye on those membranes (Fig. 6b). The rejection rate of MB on the G-T3 and G-T3-PY membranes is nearly 100%, which is higher than that of the commercial VNF1 (87.6%), VNFK (97.0%) and DK (99.7%) membranes. Interestingly, the G-T3 and G-T3-PY membranes demonstrate markedly different rejection rates toward anionic eosin dye. The G-T3 membrane has a rejection rate of only 60.5% toward eosin while G-T3-P4 shows a rejection rate of 99.5%. As mentioned above, the composite membrane becomes denser and positively charged after PEI encapsulation; it is reasonable to ascribe selective dye rejection to the different electrostatic charges of the membranes. To characterize the ion separation performance of the G-T3-P4 nanofiltration membrane, we carried out the retention experiments using four kinds of salt ions (2000 ppm $MgSO_4$, $MgCl_2$, NaCl and Na_2SO_4), the performance results of which are shown in Fig. S12.† Clearly, we can see that the average rejection rate for $MgSO_4$, $MgCl_2$, NaCl and Na_2SO_4 is 31.9, 13.8, 12.7 and 5.8%, respectively. We can conclude that the G-T3-P4 membrane shows poor performance for the rejection of salt solution but good rejection for dye solutions. Therefore, this membrane could be potentially used in the field of dye desalination and purification.

3.5 The durability of the composite membrane

Durability is another crucial index that needs to be considered. For membranes without PEI encapsulation, the dye rejection rate of G-T3 sharply drops during the second cycle, indicating that the membrane without PEI encapsulation has poor structural durability (Fig. 6c). We can see that the optimally tuned G-T3-P4 membrane with the highest surface hydrophilicity and lowest roughness shows the best flux and durability after three cycles even through operating under dry conditions, indicating it has a good mechanical integrity. Therefore, we can conclude that grafting PEI and forming a bound cortex on the membrane surface could modulate the surface properties of the membrane and thus its stability. In addition, the N element is found at a depth of 200 nm according to the XPS sputtering depth experiments (Fig. S10†), indicating that in addition to building a tightly bonded cortex on the surface, PEI also enters the interlayer of the composite membrane and cross-links the GO galleries, which further explains the stability of the NF GO membrane. G-T3-P4 with optimized MW PEI can afford a strong and stable composite membrane, which is a promising NF membrane material for potential industrial applications. For comparison, we summarize the permeance and interception rate of some typical state-of-the-art GO based NF membranes in Fig. 7 and Table S1.† Clearly, the flux of the G-T3-P4 nanofiltration membrane is 2.2 times higher than that of GO/

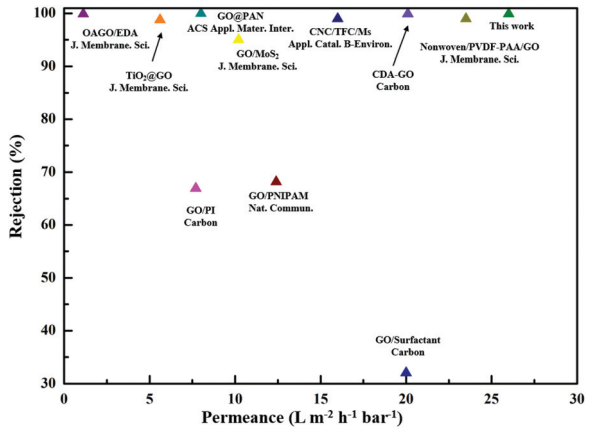

Fig. 7 Comparison of the separation performance of G-T3-P4 membrane and the state-of-the-art GO based membranes.

MoS_2.[45] We notice that the operating pressure in our case is only 1 bar, which is quite lower than that of 2 bar for the GO/MoS_2 membrane. In addition, under the same operating pressure and dye retention, the flux of the G-T3-P4 membrane is 2.34 times higher than that of the GO@PAN membrane.[48] Clearly, our G-T3-P4 membrane shows better efficiency compared to the GO based membranes toward the sieving of organic molecules in aqueous solutions.[40–49]

3.6 Separation mechanism of G-TX-PY membrane

A combination of size exclusion, charge repulsion and diffusion separation mechanism can be used to explain the separation process of the NF membranes.[50–52] The schematic diagram in Fig. 8 shows the separation mechanism of composite membranes. Clearly, water passes through the transmembrane and the interlayer pathways of the GO membranes. Introducing TiO_2 intercalants in the G-TX membrane expands the interlayer distance of the GO gallery and enables high water flux, while maintaining a high rejection of dye. For the G-TX membranes, the separation mechanism toward MB dye is the synergy of steric hindrance and electrostatic repulsion effect. Furthermore, after the cationic MB was adsorbed on the G-TX membranes, the surface forms an electric double layer, which could further enhance the rejection of the cationic dye.

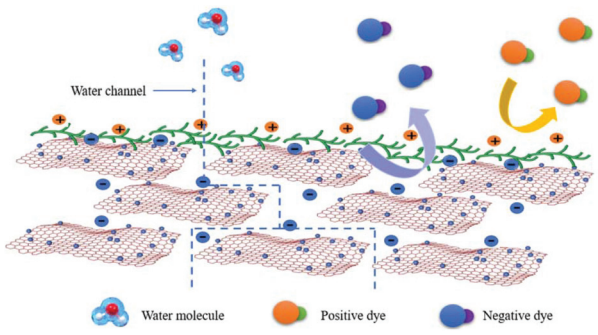

Fig. 8 Separation mechanism of GO NF composite membrane.

In addition, the rejection of MB reduced sharply (G-T4 and G-T5 samples) when the size of TiO_2 is too large, which is explained by the wider inter-layer space. Thanks to the strong electrostatic force between the negative GO layers and polycationic PEI, the membrane surface is protected by a tight PEI cortex, thus improving mechanical stability. The separation process of electropositive MB is ascribed to the electrostatic repulsion effect and size exclusion effect. As for the anionic eosin dye, positively charged PEI adsorbs the electronegative eosin, which also causes an increased steric hindrance effect.

4. Conclusions

In summary, an ultra-stable GO composite membrane was synthesized by inserting TiO_2 nanocrystals in the interlayer space and then sealing by PEI. The composite membranes exhibit good water flux and high rejection of anionic and cationic dyes. The water flux of G-T3-P4 is nearly 7 times higher than that of the commercial VNFK membrane, and its dye retention is about 99.9%. In addition, the tightly bound PEI cortex acts as a protective layer and could enhance the stability of the GO NF composite membranes. The filtration mechanism of PEI-modified NF membranes is ascribed to the steric hindrance and electrostatic charge repulsion effect. Our findings provide a viable route to fabricate GO composite nanofiltration membranes that can achieve a high-water flux and high rejection rate.

Author contributions

Z. C, Y. Q. C and K. Q. Z conceived the study and designed the experiments. K. Q. Z and S. Q. L performed the experiments. Z. C and K. Q. Z wrote the article together. W. G. L, Z. C and Y. B. H revised the article. All authors approved the article for publication.

Conflicts of interest

There are no conflicts to declare.

Acknowledgements

This work was supported by Suntar Membrane Technology (Xiamen) Co., Ltd, Xiamen.

References

1 S. Lattemann and T. Höpner, *Desalination*, 2008, **220**, 1–15.
2 J. J. Urban, *Joule*, 2017, **1**, 665–688.
3 R. Das, M. E. Ali, S. B. A. Hamid, S. Ramakrishna and Z. Z. Chowdhury, *Desalination*, 2014, **336**, 97–109.

4 J. Wang, J. Zhu, Y. Zhang, J. Liu and B. Van der Bruggen, *Nanoscale*, 2017, **9**, 2942–2957.
5 D. Cohen-Tanugi and J. C. Grossman, *Nano Lett.*, 2014, **14**, 6171–6178.
6 K. Zhao and H. Wu, *Nano Lett.*, 2015, **15**, 3664–3668.
7 R. Cruz-Silva, K. Izu, J. Maeda, S. Saito, A. Morelos-Gomez, C. Aguilar, Y. Takizawa, A. Yamanaka, S. Tejiima, K. Fujisawa, K. Takeuchi, T. Hayashi, T. Noguchi, A. Isogai and M. Endo, *Nanoscale*, 2020, **12**, 19628–19637.
8 S. Rajesh, Y. Zhao, H. Fong and T. J. Menkhaus, *Nanoscale*, 2016, **8**, 18376–18389.
9 W.-S. Hung, S.-Y. Ho, Y.-H. Chiao, C.-C. Chan, W.-Y. Woon, M.-J. Yin, C.-Y. Chang, Y. M. Lee and Q.-F. An, *Chem. Mater.*, 2020, **32**, 5750–5758.
10 C. Chi, X. Wang, Y. Peng, Y. Qian, Z. Hu, J. Dong and D. Zhao, *Chem. Mater.*, 2016, **28**, 2921–2927.
11 S. Zhao, C. Ba, Y. Yao, W. Zheng, J. Economy and P. Wang, *Chem. Eng. J.*, 2018, **335**, 101–109.
12 E. A. Jackson and M. A. Hillmyer, *ACS Nano*, 2010, **4**, 3548–3553.
13 P. K. Ang, M. Jaiswal, C. H. Y. X. Lim, Y. Wang, J. Sankaran, A. Li, C. T. Lim, T. Wohland, Ö. Barbaros and K. P. Loh, *ACS Nano*, 2010, **4**, 7387–7394.
14 S. Kim, J. Nham, Y. S. Jeong, C. S. Lee, S. H. Ha, H. B. Park and Y. J. Lee, *Chem. Mater.*, 2015, **27**, 1255–1261.
15 I. B. Valtcheva, S. C. Kumbharkar, J. F. Kim, Y. Bhole and A. G. Livingston, *J. Membr. Sci.*, 2014, **457**, 62–72.
16 P. Schmidt, E. L. Bednarz, P. Lutze and A. Górak, *Chem. Eng. Sci.*, 2014, **115**, 115–126.
17 A. Anand, B. Unnikrishnan, J.-Y. Mao, H.-J. Lin and C.-C. Huang, *Desalination*, 2018, **429**, 119–133.
18 Y. Han, Z. Xu and C. Gao, *Adv. Funct. Mater.*, 2013, **23**, 3693–3700.
19 G. Liu, W. Jin and N. Xu, *Chem. Soc. Rev.*, 2015, **44**, 5016–5030.
20 Y. Wei, Y. Zhang, X. Gao, Y. Yuan, B. Su and C. Gao, *Carbon*, 2016, **108**, 568–575.
21 A. Iakunkov and A. V. Talyzin, *Nanoscale*, 2020, **12**, 21060–21093.
22 K. Goh, W. Jiang, H. E. Karahan, S. Zhai, L. Wei, D. Yu, A. G. Fane, R. Wang and Y. Chen, *Adv. Funct. Mater.*, 2015, **25**, 7348–7359.
23 X. Chen, M. Qiu, H. Ding, K. Fu and Y. Fan, *Nanoscale*, 2016, **8**, 5696–5705.
24 S. J. Gao, H. Qin, P. Liu and J. Jin, *J. Mater.Chem. A*, 2015, **3**, 6649–6654.
25 W.-S. Hung, C.-H. Tsou, M. De Guzman, Q.-F. An, Y.-L. Liu, Y.-M. Zhang, C.-C. Hu, K.-R. Lee and J.-Y. Lai, *Chem. Mater.*, 2014, **26**, 2983–2990.
26 L. Chen, N. Li, Z. Wen, L. Zhang, Q. Chen, L. Chen, P. Si, J. Feng, Y. Li, J. Lou and L. Ci, *Chem. Eng. J.*, 2018, **347**, 12–18.
27 Y. Ying, D. Liu, W. Zhang, J. Ma, H. Huang, Q. Yang and C. Zhong, *ACS Appl. Mater. Interfaces*, 2017, **9**, 1710–1718.
28 F. Yang, M. Wu, Y. Wang, S. Ashtiani and H. Jiang, *ACS Appl. Mater. Interfaces*, 2019, **11**, 990–997.
29 Y. Xu, G. Peng, J. Liao, J. Shen and C. Gao, *J. Membr. Sci.*, 2020, **601**, 117727.
30 P. Sun, Q. Chen, X. Li, H. Liu, K. Wang, M. Zhong, J. Wei, A. Wu, R. Ma, T. Sasaki and H. Zhu, *NPG Asia Mater.*, 2015, **7**, e162.
31 L. Chen, G. Shi, J. Shen, B. Peng, B. Zhang, Y. Wang, F. Bian, J. Wang, D. Li, Z. Qian, G. Xu, G. Liu, J. Zeng, L. Zhang, Y. Yang, G. Zhou, M. Wu, W. Jin, J. Li and H. Fang, *Nature*, 2017, **550**, 380–383.
32 M.-Y. Lim, Y.-S. Choi, J. Kim, K. Kim, H. Shin, J.-J. Kim, D. M. Shin and J.-C. Lee, *J. Membr. Sci.*, 2017, **521**, 1–9.
33 C. Xu, A. Cui, Y. Xu and X. Fu, *Carbon*, 2013, **62**, 465–471.
34 J. Wang, Y. Wang, Y. Zhang, A. Uliana, J. Zhu, J. Liu and B. Van der Bruggen, *ACS Appl. Mater. Interfaces*, 2016, **8**, 25508–25519.
35 Y. Guo, X. Yang, K. Ruan, J. Kong, M. Dong, J. Zhang, J. Gu and Z. Guo, *ACS Appl. Mater. Interfaces*, 2019, **11**, 25465–25473.
36 L. Shao, X. Cheng, Z. Wang, J. Ma and Z. Guo, *J. Membr. Sci.*, 2014, **452**, 82–89.
37 J. S. Lee, K. H. You and C. B. Park, *Adv. Mater.*, 2012, **24**, 1084–1088.
38 J. Guo, H. Bao, Y. Zhang, X. Shen, J.-K. Kim, J. Ma and L. Shao, *J. Membr. Sci.*, 2021, **619**, 118791.
39 M. Safarpour, A. Khataee and V. Vatanpour, *J. Membr. Sci.*, 2015, **489**, 43–54.
40 J. Wang, Y. Wang, J. Zhu, Y. Zhang, J. Liu and B. Van der Bruggen, *J. Membr. Sci.*, 2017, **533**, 279–288.
41 J. Liu, N. Wang, L. J. Yu, A. Karton, W. Li, W. Zhang, F. Guo, L. Hou, Q. Cheng, L. Jiang, D. A. Weitz and Y. Zhao, *Nat. Commun.*, 2017, **8**, 2011.
42 B. Li, Y. Cui, S. Japip, Z. Thong and T.-S. Chung, *Carbon*, 2018, **130**, 503–514.
43 F. Baskoro, C.-B. Wong, S. R. Kumar, C.-W. Chang, C.-H. Chen, D. W. Chen and S. J. Lue, *J. Membr. Sci.*, 2018, **554**, 253–263.
44 Q. Zhang, S. Chen, X. F. Fan, H. G. Zhang, H. T. Yu and X. Quan, *Appl. Catal., B*, 2018, **224**, 204–213.
45 P. Zhang, J.-L. Gong, G.-M. Zeng, B. Song, W. Cao, H.-Y. Liu, S.-Y. Huan and P. Peng, *J. Membr. Sci.*, 2019, **574**, 112–123.
46 H. Lin, S. Dangwal, R. Liu, S.-J. Kim, Y. Li and J. Zhu, *J. Membr. Sci.*, 2018, **563**, 336–344.
47 B. Lian, J. Deng, G. Leslie, H. Bustamante, V. Sahajwalla, Y. Nishina and R. K. Joshi, *Carbon*, 2017, **116**, 240–245.
48 J. Q. Wang, P. Zhang, B. Liang, Y. X. Liu, T. Xu, L. F. Wang, B. Cao and K. Pan, *ACS Appl. Mater. Interfaces*, 2016, **8**, 6211–6218.
49 Y. Qian, C. Zhou and A. Huang, *Carbon*, 2018, **136**, 28–37.
50 S. S. Madaeni and E. Salehi, *Chem. Eng. J.*, 2009, **150**, 114–121.
51 T. Yang, H. Lin, K. P. Loh and B. Jia, *Chem. Mater.*, 2019, **31**, 1829–1846.
52 A. Gogoi, K. A. Reddy and P. K. Mondal, *Nanoscale*, 2020, **12**, 7273–7283.

